Available online at www.sciencedirect.com

ScienceDirect

IFAC PapersOnline CONFERENCE PAPER ARCHIVE

IFAC PapersOnLine 58-18 (2024) 194–199

On the Stability of Nonlinear Model Predictive Control for 3D Target Tracking

Ignacio J. Torres * **Ricardo P. Aguilera** * **Quang P. Ha** *

* *University of Technology Sydney, Ultimo, NSW, 2007, Australia*
e-mail: itorres@ieee.org, raguilera@ieee.org, quang.ha@uts.edu.au

Abstract: In this study, we present the stability analysis of a Nonlinear Model Predictive Control (NMPC) of a 3D ground target tracking system model. The system model is derived considering the 3D kinematic system model referenced to the ground target. The NMPC adeptly track errors across five states: range, bearing angle, altitude, pitch angle, and speed. This objective is achieved through the utilization of yaw angle, pitch angle, and acceleration as control inputs. The contribution of this paper is the establishment of stability conditions within the Lyapunov framework for the closed-loop system. To demonstrate the efficacy of our proposed model, we conducted simulations, which shows high accuracy in tracking all designated states.

Keywords: Fixed wings UAVs, NMPC, Stability, Target Tracking.

1. INTRODUCTION

Unmanned Aerial Vehicles (UAVs) have emerged as pivotal technological assets, finding applications across diverse sectors such as agriculture, search and rescue, and military operations (Wilson et al., 2022). Within the realm of UAV technology, quadcopters and fixed-wing platforms present distinctive advantages and challenges (Attenni et al., 2023; Tahir et al., 2023; Zuo et al., 2022). While fixed-wing UAVs boast enhanced autonomy and extended range, they grapple with a fundamental constraint: the inability to maintain stationary flight, necessitating continuous motion.

In the context of ground target tracking with fixed-wing UAVs, the prevalent strategies involve overhead tracking or circumnavigation of specified targets at predefined distances (Chen et al., 2019). Achieving this involves skillful manipulation of circumnavigation angles to control direction and maintain desired distances, often implemented through a 2D Dubins model but with 3D implementation as well (Mbam and Kim, 2023).

Model Predictive Control (MPC) has gained prominence in control theory due to its efficacy in addressing control problems while accounting for system constraints (Mayne, 2014). Traditional MPC methodologies rely on linear approximations of systems, leading to well-studied convex optimization problems with distinct global optimal solutions (Rawlings, 2000). However, Nonlinear MPC needs to deal with nonconvex optimization, posing challenges in finding global optimum solutions due to nonlinearities in the dynamic system model (Wolf and Marquardt, 2016).

Ensuring stability in MPC systems often hinges on Lyapunov theory, where the selection of a Candidate Lyapunov Function (CLF) within specific bounds plays a crucial role. In linear applications, stability is attained by adding a properly design terminal cost into the cost function by solving the algebraic Riccati equation (Wei, 2021).

In recent years, NMPC applied to fixed-wings has gain prominence. Authors at (Reinhardt and Johansen, 2021) propose an NMPC for attitude and speed control for fixed-wings. Moreover, at (Tian et al., 2022), authors proposed a double-layer fuzzy adaptive NMPC for trajectory tracking and energy management control. Notwithstanding these developments, a number of unresolved issues still need to be addressed, stability being prominent among them.

This paper presents the stability analysis of a NMPC approach to control a 3D ground target tracking model. Based on the 3D kinematics system model, a 5-states and 3-inputs target tracking system model is derived. With this, a local controller is design that stabilizes the system within the terminal region. Sufficient conditions of stability are given, and simulation results shows the good performance of the controller on tracking the system states' references.

The structure of this paper unfolds as follows: Section 2 establishes foundational elements pertinent to this study Subsequently, Section 3 expounds on the system's dynamic model using kinematics, leading to the derivation of the ground target tracking model. Section 4 details the application of nonlinear Model Predictive Control within this system. The stability analysis is discussed in Section 5. Section 6 presents simulation results, and section 7 encapsulates the conclusions and outlines avenues for future exploration.

NOTATION

In this work, $\mathbb{R}$ signifies the set of all real numbers, whereas $\mathbb{R}_+$ refers to the set of all non-negative real numbers. We use $A^\intercal$ to indicate the transpose of a matrix A. For a matrix A, its largest and smallest eigenvalues are represented by $\lambda_{\max}(A)$ and $\lambda_{\min}(A)$, respectively. The largest singular value of a matrix A is its induced norm.

10.1016/j.ifacol.2024.09.030

The Euclidean norm is expressed as $|\cdot|$. Furthermore, the weighted squared Euclidean norm is given by the expression $|x|_P^2 = x^\intercal P x$.

2. PRELIMINARIES

Take into account the following discrete-time autonomous system model:

$$x_{k+1} = f(x_k), \qquad f(0) = 0, \tag{1}$$

where $x_k \in \mathbb{R}^n$.

Definition 1. $\mathcal{K}$ and $\mathcal{KL}$ Functions: If a function $\alpha : \mathbb{R}_+ \to \mathbb{R}+$ is continuous, monotonically increasing, and fulfills $\alpha(0) = 0$, it is categorized as a $\mathcal{K}$-function. Additionally, if α is a $\mathcal{K}$-function with the feature that $\alpha(a) \to \infty$ as $a \to \infty$, then it is regarded as a $\mathcal{K}_\infty$-function. On the other hand, a function $\beta : \mathbb{R}_+ \times \mathbb{R}_+ \to \mathbb{R}_+$ is recognized as a $\mathcal{KL}$-function if it is continuous, $\beta(\cdot, k)$ is a $\mathcal{K}$-function for all $k \geq 0$, and $\beta(s, \cdot)$ is a non-increasing function for all $s \geq 0$, with $\beta(s, k) \to 0$ as $k \to \infty$.

Definition 2. (Lyapunov Stability): For the system (1), a function $V : \mathbb{R}^n \to \mathbb{R}$ is identified as a Lyapunov function within a subset $\mathcal{A} \subset \mathbb{R}^n$ if, within $\mathcal{A}$, there is a compact set Ω, encompassing the neighborhood around the origin $x = 0$, $\mathcal{K}_\infty$-functions α_1, α_2, and α_3 meeting the following criteria:

$$V(x) \geq \alpha_1(|x|), \forall x \in \mathcal{A}, \tag{2a}$$
$$V(x) \leq \alpha_2(|x|), \forall x \in \Omega, \tag{2b}$$
$$V(f(x)) - V(x) = \Delta V(x) \leq -\alpha_3(|x|), \forall x \in \mathcal{A}. \tag{2c}$$

When $\mathcal{A} \triangleq \mathbb{R}^n$, V is regarded as a global Lyapunov function.

Theorem 1. (Limon et al. (2009)). If the system (1) admits a Lyapunov function in $\mathcal{A}$, then it is asymptotically stable in $\mathcal{A}$.

3. 3D GROUND TARGET TRACKING SYSTEM MODEL

The system model introduced in this study takes into account the kinematic relationship between the fixed-wing UAV and a spatial location, with a specific focus on a ground target as the reference point. Within this context, we assume precise knowledge of the target's positional coordinates. The continuous-time kinematic representation of the fixed-wing UAV concerning the ground target can be denoted as follows:

$$\dot{x}_p = v\cos(\chi)\cos(\psi), \tag{3a}$$
$$\dot{y}_p = v\cos(\chi)\sin(\psi), \tag{3b}$$
$$\dot{z}_p = v\sin(\chi), \tag{3c}$$
$$\dot{\chi} = u_\chi, \tag{3d}$$
$$\dot{\psi} = u_\psi, \tag{3e}$$
$$\dot{v} = u_v. \tag{3f}$$

In this conceptual framework, x_p, y_p, and z_p represent the spatial coordinates of the UAV in a three-dimensional context. Additionally, v denotes the UAV's speed, while χ and ψ respectively represent the pitch and heading angles of the UAV (Zhang et al., 2018). Moreover, the control inputs, namely u_χ, u_ψ, and u_v, govern the rates of change for the pitch angle (χ), heading angle (ψ), and speed (v). These control inputs are pivotal in orchestrating the UAV's maneuvers and ensuring effective ground target tracking. The UAV's operational dynamics necessitate the generation of adequate lift for sustained flight. Consequently, the UAV's speed v is confined within the interval $[v_{\min}, v_{\max}]$. Here, $v_{\max}$ denotes the maximum attainable speed for the UAV, while $v_{\min}$ corresponds to the stall speed, which is the minimum speed required to sustain lift.

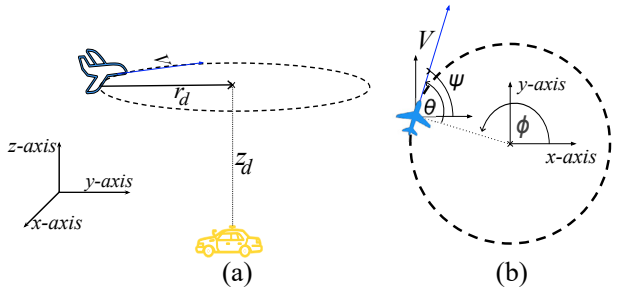

Fig. 1. a) 3D Ground Target Tracking. (b) XY representation for angles relationship.

3.1 Nonlinear 3D Ground Target Tracking System Model

Considering the Fig. 1b, the relationship between the bearing angle, heading angle, and reference angle from the ground target and the UAV is depicted as:

$$\phi = \psi - \theta - \pi, \tag{4}$$

with $\phi = \arctan 2(y_p, x_p)$, (4) implies $\dot{\phi} = \dot{\psi} - \dot{\theta}$. Moreover, from Fig. 1a the distance between the UAV and the target tracking is represented by:

$$r(t) = \sqrt{(x_p(t) - x_{GT})^2 + (y_p(t) - y_{GT})^2} \tag{5}$$

where x_{GT}, y_{GT} are the ground target position coordinates. For simplicity, $x_{GT} = y_{GT} = 0$, i.e. the ground target is at the origin of the 3D frame. Furthermore, the derivative of the distance $\dot{r}$ can be depicted as:

$$\dot{r} = \frac{1}{2\sqrt{x_p^2 + y_p^2}}\left(2x_p\dot{x_p} + 2y_p\dot{y_p}\right) \tag{6}$$

Additionally, from (4),

$$\dot{\phi} = \frac{-y_p}{x_p^2 + y_p^2}\dot{x}_p + \frac{x_p}{x_p^2 + y_p^2}\dot{y}_p = \frac{-v\cos\chi\cos\theta}{r}, \tag{7}$$

Considering the rate of change of the altitude $\dot{z}_p$, the rate of change of the speed $\dot{v}$, the rate of change of the pitch angle $\dot{\chi}$ at (3), and by (4), (6) and (7), the 3D target tracking model is depicted as:

$$\dot{r} = -v\cos\chi\cos\theta, \tag{8a}$$
$$\dot{\theta} = \frac{v\sin\theta\cos\chi}{r} + u_\psi, \tag{8b}$$
$$\dot{z}_p = v\sin(\chi), \tag{8c}$$
$$\dot{\chi} = u_\chi, \tag{8d}$$
$$\dot{v} = u_v. \tag{8e}$$

The steady-state analysis shows that, while $v \geq v_{min}$, if $\dot{r} = \dot{\theta} = \dot{z}_p = \dot{\chi} = \dot{v} = 0 \implies \chi_{ss} = u_{\chi,ss} = u_{v,ss} = 0$, $\theta_{ss} = \{\pi/2, -\pi/2\}$, $u_{\psi,ss} = \{-v_{ss}/r_{ss}, v_{ss}/r_{ss}\}$. The subsequent states tracking error vector is defined as $x = \bar{x} - x_{ss}$, where $\bar{x} = [r\ \theta\ z_p\ \chi\ v]^\intercal$ is the actual state value vector and $x_{ss} = [r_{ss}\ \theta_{ss}\ z_{p,ss}\ \chi_{ss}\ v_{ss}]^\intercal$ is the reference vector. Similarly to the states, the inputs tracking error vector is defined as $u = \bar{u} - u_{ss}$,

where $\bar{u} = [u_\psi \ u_\chi \ u_v]^\intercal$ is the actual inputs vector, and $u_{ss} = [u_{\psi,ss} \ u_{\chi,ss} \ u_{v,ss}]^\intercal$ represents the steady-state input vector. Considering forward Euler method for discretization and tracking errors, we can represent the model as a discrete-time tracking error form nonlinear system model as follows:

$$x_{k+1} = h(x_k) + Bu_k, \tag{9}$$

where

$$B = \begin{bmatrix} 0 & 0 & 0 \\ T_s & 0 & 0 \\ 0 & 0 & 0 \\ 0 & T_s & 0 \\ 0 & 0 & T_s \end{bmatrix},$$

and $h(x_k) = [h_1 \ h_2 \ h_3 \ h_4 \ h_5]^\intercal$ defined by:

$$h_1(x_k) = x_{1k} + T_s(x_{5k}+v_{ss})(\sin x_{2k} \cos x_{4k}), \tag{10a}$$

$$h_2(x_k) = x_{2k} + T_s \left(\frac{(x_{5k}+v_{ss}) \cos x_{4k} \cos x_{2k}}{(x_{1k}+r_{ss})} - \frac{v_{ss}}{r_{ss}} \right), \tag{10b}$$

$$h_3(x_k) = x_{3k} + T_s(x_{5k}+v_{ss}) \sin x_{4k}, \tag{10c}$$

$$h_4(x_k) = x_{4k}, \tag{10d}$$

$$h_5(x_k) = x_{5k}, \tag{10e}$$

where T_s is the sampling time. Note that the sub index k denotes sampling instant.

3.2 Linearized 3D Ground Target Tracking System Model

Considering the nonlinear system presented in (9), and the linearization point as $x_{ss} = [r_{ss} \ \pi/2 \ z_{p,ss} \ 0 \ v_{ss}]^\intercal$, we can obtain a linearized representation of the discrete-time system model for the ground target tracking system as

$$x_{k+1} = Ax_k + Bu_k, \tag{11}$$

with

$$A = \begin{bmatrix} 1 & T_s v_{ss} & 0 & 0 & 0 \\ 0 & 1 & 0 & 0 & \frac{T_s}{r_{ss}} \\ 0 & 0 & 1 & T_s v_{ss} & 0 \\ 0 & 0 & 0 & 1 & 0 \\ 0 & 0 & 0 & 0 & 1 \end{bmatrix}.$$

Moreover, the nonlinear system can be represented as:

$$f(x_k, u_k) = Ax_k + Bu_k + g(x_k), \tag{12}$$

where the discrepancy between the linear and nonlinear system models is denoted by $g(x_k) = h(x_k) - Ax_k$. The linear and nonlinear models become increasingly similar as the states get closer to their references, meaning that the gap between them tends to zero at this stage.

4. FORMULATION OF NMPC FOR 3D GROUND TARGET TRACKING

In this section, we consider the discrete-time model for ground target tracking as specified in (9), where the state x_k and control input u_k are elements of $\mathbb{R}^n$ and $\mathbb{R}^m$, respectively. The primary goal is to minimize the cost function described by:

$$V_N(x_0, \overrightarrow{u}) = \sum_{i=0}^{N-1} L(x_i, u_i) + V_f(x_N), \tag{13}$$

with the stage cost is expressed as $L(x_i, u_i) = |x_i|^2_Q + |u_i|^2_R$, where Q and R are positive definite matrices. The prediction horizon is denoted by N. The terminal cost is defined as $V_f(x_N) = |x_N|^2_{P_\rho}$ with P_ρ being a positive definite matrix. Given tentative inputs u_k over N, the sequence of control actions $\overrightarrow{u}$ is as follows:

$$\overrightarrow{u} = [(u_0)^\intercal \ \dots \ (u_{N-1})^\intercal] \in \mathbb{R}^{m \times N}. \tag{14}$$

The NMPC problem for the initial state x_0 is formulated as an optimal control problem as follows:

$$\mathbb{P}_N(x_0) : V_N^{opt}(x_0, \overrightarrow{u}) = \min_{\overrightarrow{u}} V_N(x_0, \overrightarrow{u}), \tag{15a}$$

$$\text{s.t.:}$$

$$x_{i+1} = f(x_i, u_i), \tag{15b}$$

$$u_i \in \mathbb{U}, \tag{15c}$$

$$x_i \in \mathbb{R}^n, \tag{15d}$$

$$x_N \in \mathbb{X}_f \subseteq \mathbb{R}^n, \tag{15e}$$

$$\forall i \in \{0, \cdots, N-1\}.$$

The constraints (15b) and (15c) correspond to the system and input constraints, respectively, while (15e) is the terminal constraint, allowing the design of $\mathbb{X}_f$ to ensure closed-loop stability. The optimal input vector $\overrightarrow{u}^{opt}$ that minimizes the cost function (13) is defined as:

$$\overrightarrow{u}^{opt}(x_0) \equiv \arg \left\{ \min_{\overrightarrow{u} \in \mathcal{U}(x_0)} V_N(x_0, \overrightarrow{u}) \right\}. \tag{16}$$

The set of feasible control actions that adhere to constraints (15c) to (15e) is indicated by $\mathcal{U}(x)$. Thus, the optimal input sequence is stated as follows:

$$\overrightarrow{u}^{opt}(x_0) = \left[(u_0^{opt})^\intercal \ \dots \ (u_{N-1}^{opt})^\intercal \right]^\intercal. \tag{17}$$

Implementing $\overrightarrow{u}^{opt}(x_0)$ in the system (15b) results in the optimal state trajectory:

$$\overrightarrow{x}^{opt}(x_0) = \left[(x_0)^\intercal \ (x_1^{opt})^\intercal \ \dots \ (x_N^{opt})^\intercal \right]^\intercal. \tag{18}$$

Then, it is possible to define the domain of attraction for $V_N(x_0)$ as follows

$$X_N \equiv x_0 \in \mathbb{R} : \mathcal{U}(x_0) \neq \emptyset, \tag{19}$$

comprising all $x_0 \in \mathbb{R}^n$ for which there is an input sequence $\overrightarrow{u} \in \mathcal{U}(x_0)$ holding the constraints (15c) through (15e). By employing the receding horizon control principle, solving $\mathbb{P}_N(x_0)$ in (15a) determines the NMPC law $\kappa_N(x_k) : X_N \to \mathbb{U}$:

$$\kappa_N(x_0) \equiv u_0^{opt}. \tag{20}$$

Lastly, considering (12), the NMPC loop for tracking a ground target is denoted as:

$$x_{k+1} = f(x_k, \kappa_N(x_k)). \tag{21}$$

5. STABILITY ANALYSIS

Here we focus on deriving sufficient conditions for the NMPC loop's stability in UAV ground target tracking, outlined in (21). Although the purpose of this analysis is to ensure closed loop NMPC stability for the ground target tracking system, we use standard linear tools to derive sufficient stability conditions.

5.1 Terminal Local Controller $\kappa_\ell(x)$

A standard method for assuring stability in NMPC involves the use of a known controller, which stabilizes the nonlinear system at $x \in \mathbb{X}_f$. Drawing inspiration from this approach and utilizing conventional linear MPC tools, coupled with the behavior of $g(x)$ approaching zero as x approaches zero, we propose a local controller based on

the characteristics of the optimal solution for a one-step horizon (i.e., $N = 1$) (Aguilera et al., 2013) with $\rho = 1$. The local controller is thus defined:

$$\kappa_\ell(x) = Kx, \tag{22}$$

where

$$K = -(B^\intercal PB + R)^{-1}B^\intercal PA. \tag{23}$$

In light of this and the terminal cost, $\mathbb{X}_f$ in (15e) is defined as follows:

$$\mathbb{X}_f \triangleq \{x^\intercal P_\rho x \leq \varrho_x : \kappa_\ell(x) \in \mathbb{U}\}, \tag{24}$$

where ϱ_x is a positive real number chosen to maximize the ellipsoid size such that for all x within the terminal region, $\kappa_\ell(x)$ remains within $\mathbb{U}$ in (12). Additionally, as the origin is included in $\mathbb{U}$, this ensures $\mathbb{X}_f$ is non-empty. Regarding (12), the closed-loop system can be represented as:

$$x_{k+1} = A_K x_k + g(x_k), \tag{25}$$

with $A_K = A + BK$. Considering $g(\cdot)$ to be twice differentiable and satisfying $g(0) = 0$, there is a positive real constant $\mathcal{L}$ that can be used in the following relationship:

$$|g(x)| \leq \mathcal{L}|x|, \tag{26}$$

on the subset $\mathbb{X}_f \subset \mathbb{R}^n$, signifying that $g(x)$ is locally Lipschitz within $\mathbb{X}_f$.

Theorem 2. Considering the positive constants: $a_1 = \lambda_{\min}(P)$, $a_2 = \lambda_{\max}(P)$, $b = 2\mathcal{L}|A_K|_{P_\rho} + \mathcal{L}^2$ and $\sigma = \lambda_{\min}(Z^*)$, with $Z^* = {P_\rho}^{-1/2}(Q^*){P_\rho}^{-1/2}$. Moreover, $Q^* \triangleq Q + K^\intercal RK$, and $Q^*_\rho \equiv \rho Q^*$ with $\rho \geq 1$. If V_f in (13) is designed such that P_ρ solves the Riccati equation:

$$A_K^\intercal P_\rho A_K - P_\rho + Q^*_\rho = 0, \tag{27}$$

and $g(x)$ is limited as shown in (26), alongside the condition

$$\rho\sigma \geq b, \tag{28}$$

then $\kappa_\ell(x)$ in (22) acts as a local stabilizer controller within the terminal region for the system (9).

Proof. By invoking Theorem 1, the first two conditions are met with $\alpha_1(s) = a_1 s^2$ and $\alpha_2(s) = a_2 s^2$. This confirms that inequalities (2a) and (2b) are satisfied for all $x \in \mathbb{X}_f$. Continuing with direct computation, we arrive at:

$$\begin{aligned}&\Delta V_f(x_k) + L(x_k, \kappa_\ell(x_k)) = \\ &- x_k^\intercal(Q^*_\rho - Q^*)x_k + 2g(x_k)^\intercal P_\rho A_K x_k + g(x_k)^\intercal P_\rho g(x_k).\end{aligned} \tag{29}$$

Noting (26) and letting $x_k = x$, $\mathcal{L}$ can be determined by assessing $|x|_{P_\rho}$ within $\mathbb{X}_f$ and identifying its upper bound, as shown:

$$\mathcal{L} = \max_{0<|x|_{P_\rho}\leq\varrho_x} \frac{|g(x)|_{P_\rho}}{|x|_{P_\rho}}, \tag{30}$$

which implies that

$$g(x)^\intercal P_\rho g(x) \leq \mathcal{L}^2|x|^2_{P_\rho}. \tag{31}$$

Moreover

$$\begin{aligned}2g(x)^\intercal P_\rho A_K x &= 2(g(x)^\intercal {P_\rho}^{1/2})({P_\rho}^{1/2}A_K x), \\ &\leq 2\mathcal{L}|A_K|_{P_\rho}|x|^2_{P_\rho}.\end{aligned} \tag{32}$$

Similarly to (32)

$$x^\intercal(Q^*)x \geq \sigma|x|^2_{P_\rho}. \tag{33}$$

Consequently, from (29), the following is inferred:

$$\Delta V_f(x) + L(x_k, \kappa_\ell(x)) \leq -((\rho-1)\sigma - b)|x|^2_{P_\rho}, \tag{34}$$

therefore,

$$\Delta V_f(x) \leq -(\rho\sigma - b)|x|^2_{P_\rho}. \tag{35}$$

Condition (2c) is held with $\alpha_3(s) = a_3 s^2$ by (28), where

$$a_3 = (\rho\sigma - b),$$

following that

$$\Delta V_f(x) \leq -a_3|x|^2_{P_\rho}, \quad \forall x \in \mathbb{X}_f. \tag{36}$$

The previous result allows us to establish the following relationship:

$$V_f(x_{k+1}) \leq \gamma V_f(x_k), \quad \forall x \in \mathbb{X}_f. \tag{37}$$

Considering inequality (36),

$$V_f(x_{k+1}) \leq V_f(x_k) - a_3|x_k|^2_{P_\rho} \leq (a_2 - a_3)|x_k|^2_{P_\rho}, \tag{38}$$

with $a_3 \leq a_2 \implies \gamma = 1 - a_3/a_2 \in [0, 1]$. By iterating (37), it is possible bound $|x_k|^2_{P_\rho}$ as:

$$|x_k|^2 \leq \frac{a_2}{a_1}\gamma^k|x_0|^2, \tag{39}$$

implying that $\lim_{k\to\infty}|x_k| = 0$ with $x_0 \in \mathbb{X}_f$. Consequently, $\kappa_\ell(x)$ in (22) is a stabilizing local controller within the terminal region for (12).

Remark 1. The conclusions drawn from Theorem 2 indicate that under the condition where (28) is fulfilled within the set $\mathbb{U}$, the single-step controller defined in (22) effectively ensures local stability within the region $\mathbb{X}_f$. This implies that if a state x_k lies in $\mathbb{X}_f$, then its successor state x_{k+1} will also reside in $\mathbb{X}_f$, thereby rendering $\mathbb{X}_f$ as an invariant set. These insights are pivotal for the formulation of Theorem 3, which aims to establish the stability criteria for the multi-step NMPC.

5.2 Stability Analysis for Multi-step NMPC

Under the direction of the stabilizing local controller specified in (22), this subsection explores the requirements that the multi-step NMPC loop (21) must be met in order to guarantee its stability. The main tactic is to make sure the NMPC directs the system from any initial state $x_0 \in X_N$ to the terminal region and makes sure the final x_N state predicted by the system falls inside $\mathbb{X}_f$.

Theorem 3. Considering $Z = {P_\rho}^{-1/2}(Q){P_\rho}^{-1/2}$, Z^* as per Theorem 2, and $\xi = \lambda_{\min}(Z)$. If $x_N \in \mathbb{X}_f$, P_ρ in V_f satisfies (27), and

$$b \leq (\rho - 1)\sigma + \xi, \tag{40}$$

then the stability of the system in (21) is assured

Proof. Drawing from Theorem 2, condition (2a) is satisfied if $\alpha_1(s) = a_1 s^2$. Employing the local controller $\kappa_\ell(x)$ as defined in (22), we propose a suboptimal yet feasible control sequence given by:

$$\tilde{u} = [\kappa_\ell(x)^\intercal \ \kappa_\ell(x_1)^\intercal \ \cdots \ \kappa_\ell(x_{N-1})^\intercal]^\intercal.$$

Building upon the insights from Theorem 2, we establish the following relationship:

$$|x_{N-1}|^2_Q + |\kappa_\ell(x_{N-1})|^2_R + |x_N|^2_{P_\rho} = |x_{N-1}|^2_{Q^*} + |x_N|^2_{P_\rho}. \tag{41}$$

Rewriting (41) in the context of (25), we get:

$$\begin{aligned}|x_{N-1}|^2_{Q^*} + |x_N|^2_{P_\rho} &= |x_{N-1}|^2_{Q^*} + |g(x_{N-1})|^2_{P_\rho}, \\ &+ 2g(x_{N-1})^\intercal P_\rho A_K x_{N-1} + |A_K x_{N-1}|^2_{P_\rho}.\end{aligned} \tag{42}$$

Analogous to (33), we can assert the following relationship:

$$|x_{N-1}|^2_{Q^*} \leq \eta|x_{N-1}|^2_{P_\rho}, \tag{43}$$

where $\eta = \lambda_{\max}(Z^*)$. Additionally, utilizing (31) and (32), we deduce:

$$|x_{N-1}|^2_{Q^*} + |x_N|^2_{P_\rho} \leq (\eta + \tau)|x_{N-1}|^2_{P_\rho}, \tag{44}$$

where $\tau = b + |A_K|^2_{P_\rho}$. Extending the multi-step cost function (41) to incorporate x_{N-2} and considering (44), we arrive at:

$$|x_{N-2}|^2_{Q^*} + |x_{N-1}|^2_{Q^*} + |x_N|^2_{P_\rho} \leq |x_{N-2}|^2_{Q^*} + (\eta + \tau)|x_{N-1}|^2_{P_\rho}. \quad (45)$$

With (25), x_{N-1} is expressed in terms of x_{N-2}. Proceeding with this iterative process and considering optimality, we can state:

$$V_N^{opt}(x, \overrightarrow{u}^{opt}(x)) \leq V_N(x, \tilde{u}(x)) \leq \left(\sum_{j=0}^{N-2} \eta\tau^j + \tau^{N-1} \right) |x|^2_{P_\rho}, \quad \forall x \in \mathbb{X}_f. \quad (46)$$

Consequently, $\alpha_2(s) = c_2 s^2$ holds according to (2b), with

$$c_2 = \left(\sum_{j=0}^{N-2} \eta\tau^j + \tau^{N-1} \right).$$

Given the optimal control sequence as stated in (17), the optimal cost in (13) is described by:

$$V_N^{opt}(x) = V_N(x, \overrightarrow{u}^{opt}(x)). \quad (47)$$

Taking into account the stabilizing local controller shown in (22), $\tilde{u}$ is defined as a feasible but suboptimal sequence

$$\tilde{u} = \left[(u_1^{opt})^\intercal \ \cdots \ (u_{N-1}^{opt})^\intercal \ (\kappa_\ell(x_N))^\intercal \right]^\intercal. \quad (48)$$

By constraint (15e), $x_N \in \mathbb{X}_f$, and taking into account both optimality and $\tilde{u}$:

$$V_N^{opt}(x_{k+1}) \leq V_N(x_{k+1}, \tilde{u}), \quad (49)$$

we establish the following relationship by juxtaposing both (47) and (49):

$$\Delta V_N^{opt}(x_k) \leq V_N(x_{k+1}, \tilde{u}) - V_N^{opt}(x_k) = -L(x_k, \kappa_N(x_k)) + L(x_N, \kappa_\ell(x_N)) + \Delta V_f(x_N). \quad (50)$$

In alignment with (33),

$$L(x_k, \kappa_N(x_k)) \geq \xi |x_k|^2_{P_\rho}. \quad (51)$$

Therefore, from (35),

$$\Delta V_N(x_k) \leq -(\xi + (\rho - 1)\sigma - b)|x_k|^2_{P_\rho}, \quad \forall x \in X_N, \quad (52)$$

fulfilling condition (40), (2c) is satisfied with $\alpha_3(s) = -c_3 s^2$, where

$$c_3 = \xi + (\rho - 1)\sigma - b.$$

With the previous analysis, and considering that for an instant $t > 0, x \in \mathbb{X}_f$, we obtain that

$$V_N^{opt}(x_{k+1}) \leq V_N^{opt}(x_k) - c_3 |x_k|^2_{P_\rho}. \quad (53)$$

Considering (46) and establish the following relationship:

$$V_N^{opt}(x_{k+1}) \leq \gamma_n V_N^{opt}(x_k), \quad (54)$$

with $\gamma_n = 1 - c_3/c_2 \implies \gamma_n \in [0, 1)$. By iterating (55), the cost function is bounded by:

$$V_N^{opt}(x_k) \leq \gamma_n^k V_N^{opt}(x_t), \quad (55)$$

which implies that when $k \to \infty \implies V_N^{opt} \to 0, \forall\ k > t, x \in \mathbb{X}_f$. Furthermore, by the two first conditions at (2) and iterating (55), we can establish that

$$|x_k|^2 \leq \frac{c_2}{c_3} \gamma_n^k |x_t|^2, \quad (56)$$

showing that $\lim_{k\to\infty} \|x_k\| = 0$ with $x_t \in \mathbb{X}_f$. The fixed-wing UAV system controlled by NMPC given in (21) is guaranteed to be stable after the three stability requirements in (2) are met.

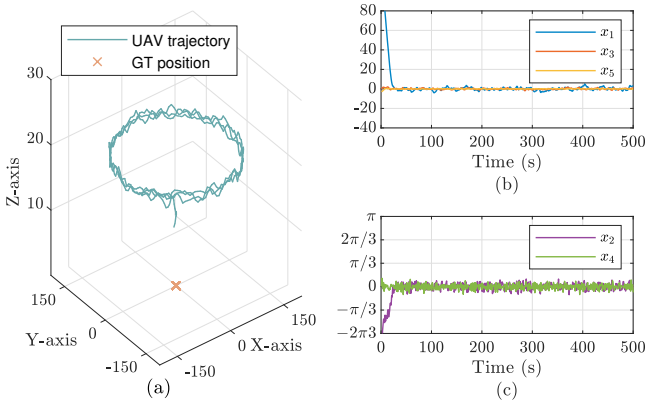

Fig. 2. Stationary Target. (a) UAV Trajectory. (b) Distance, altitude and speed tracking errors. (c) Bearing and pitch angle tracking errors.

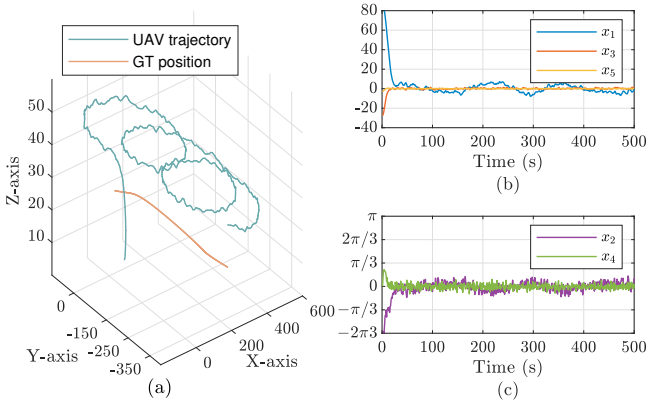

Fig. 3. Moving Target. (a) UAV and target trajectories. (b) Distance, altitude and speed tracking errors. (c) Bearing and pitch angle tracking errors.

6. SIMULATIONS

This section evaluates the NMPC system's performance by simulating its behavior in a controlled environment. The pivotal system parameters employed in these simulations are enumerated in Table 1. The system parameters can be observed in Table 1. Considering the weighting factors as

$$Q = \text{diag}([0.008, 1, 0.05, 1, 1]), \quad R = \text{diag}([1, 1, 1]), \quad (57)$$

matrices P and K can be designed solving algebraic Riccati equation at (27). Furthermore, with $\rho = 1.1$, so Q_ρ^* is determined. The design of this local controller allows the design of the terminal region $\mathbb{X}_f$, as per (58),

Table 1. System and Controller Parameters

Parameter	Symbol	Value	Units
Reference range	r_{ss}	150	m
Reference altitude	z_{ss}	20	m
Reference speed	v_{ss}	6	m/s
Reference bearing angle	θ_{ss}	$\pi/2$	$rads$
Sampling time	T_s	1	s
Simulation time	T_{sim}	500	s
Terminal region	$\mathbb{X}_f$	1.0414	-
Scaling factor	ρ	1.1	-
Prediction horizon	N	10	-
Lipschitz constant	$\mathcal{L}$	0.0372	-

$$\mathbb{X}_f = \{x^\intercal P_\rho x \leq \varrho_x = 1.0414\}. \quad (58)$$

Aligned with Theorem 3, the Lipschitz constant that bounds the nonlinearities is defined as $\mathcal{L} = 0.0372$. Finally, under condition (40), the system's stability is verified:

$$\xi + (\rho - 1)\sigma = 0.1524 > 2\mathcal{L}\|A_K\|_{P_\rho} + \mathcal{L}^2 = 0.1387.$$

For simulation purposes, two scenarios are considered. The UAV initial condition for both cases is $x_o = [282.83\ \ -\pi/4\ \ 20\ \ 0\ \ 0]^\intercal$. Figure 2. The first scenario depicts wherein the target remains stationary. Figure 2a illustrates the trajectory over the course of the simulation. It is evident that the UAV successfully attains the desired altitude before achieving and sustaining the required proximity to the target. Moreover, Figure 2b demonstrates the deviations in system states. It is apparent that within 30 seconds, the UAV aligns with the altitude reference, followed sequentially by range and speed alignment. Furthermore, Figure 2c depicts the progression of the bearing and pitch angles. Consistent with earlier observations, these two states converge to their respective references, maintaining minimal error margins, which highlights the controller's performance.

On the second case, we consider a moving target. Figure 3a showcases the trajectories of the UAV and the moving target, where the tracking of the target is achieved, maintaining a direction and remaining at the desired altitude and distance. Similarly as the stationary target case, Figure 3b and 3c show the evolution of the states throughout the simulation. Around the 30-second mark, the NMPC is able to steer the system to the references and remaining it around the references. An interesting observation is that, on the contrary as the stationary target case, the system present oscillations around the references values. This is due to the moving nature of the target, which constantly steer the states away from their reference values. Nevertheless, the controller is able to steer the system back to the references and remain that oscillations confined.

7. CONCLUSION

This paper presents the stability analysis of a NMPC specifically tailored for fixed-wing UAV engaged in precise three-dimensional ground target tracking. The proposed NMPC framework, governing five state variables and three control inputs, ensures system stability while effectively accounting for the distinctive attributes of these UAVs, particularly through consideration of input constraints. The proposed stability analysis relies on the design of a suitable local stabilizing controller within a terminal region. Simulations results were conducted for a ground target tracking problem, the NMPC cost function was design in order to satisfy the sufficient stability conditions proposed in this work. These results shows that the system is stable, moreover, a good performance is achieved, were the state variables remains within negligible error margins. Future research directions include enhancing the robustness of the proposal against model inaccuracies, conducting experiments in real-world settings, and exploring advanced computational strategies for efficiently addressing complex nonconvex optimization problems.

REFERENCES

Aguilera, R.P., Lezana, P., and Quevedo, D.E. (2013). Finite-control-set model predictive control with improved steady-state performance. *IEEE Trans. Ind. Informat.*, 9(2), 658–667.

Attenni, G., Arrigoni, V., Bartolini, N., and Maselli, G. (2023). Drone-based delivery systems: A survey on route planning. *IEEE Access*, 11, 123476–123504.

Chen, J., Zhang, W., Wang, S., Li, Y., and Wang, K. (2019). Ground target guidance method for oriented overhead tracking of fixed-wing uav. In *2019 IEEE International Conference on Power, Intelligent Computing and Systems (ICPICS)*, 1–5.

Limon, D., Alamo, T., Raimondo, D.M., de la Peña, D.M., Bravo, J.M., Ferramosca, A., and Camacho, E.F. (2009). *Input-to-State Stability: A Unifying Framework for Robust Model Predictive Control*, 1–26. Springer Berlin Heidelberg, Berlin, Heidelberg.

Mayne, D.Q. (2014). Model predictive control: Recent developments and future promise. *Automatica*, 50(12), 2967–2986.

Mbam, C.J. and Kim, J. (2023). Optimal tracking & evasive algorithms for fixed-wing uav & target in 3-dimensional space. *IFAC-PapersOnLine*, 56(2), 4527–4532. 22nd IFAC World Congress.

Rawlings, J. (2000). Tutorial overview of model predictive control. *IEEE Control Systems Magazine*, 20(3), 38–52.

Reinhardt, D. and Johansen, T.A. (2021). Control of fixed-wing uav attitude and speed based on embedded nonlinear model predictive control. *IFAC-PapersOnLine*, 54(6), 91–98. 7th IFAC Conference on Nonlinear Model Predictive Control NMPC 2021.

Tahir, M.A., Mir, I., and Islam, T.U. (2023). A review of uav platforms for autonomous applications: Comprehensive analysis and future directions. *IEEE Access*, 11, 52540–52554.

Tian, W., liu, L., Zhang, X., and Yang, D. (2022). Double-layer fuzzy adaptive nmpc coordinated control method of energy management and trajectory tracking for hybrid electric fixed wing uavs. *International Journal of Hydrogen Energy*, 47(92), 39239–39254.

Wei, Y. (2021). Lyapunov stability theory for nonlinear nabla fractional order systems. *IEEE Transactions on Circuits and Systems II: Express Briefs*, 68(10), 3246–3250.

Wilson, A.N., Kumar, A., Jha, A., and Cenkeramaddi, L.R. (2022). Embedded sensors, communication technologies, computing platforms and machine learning for uavs: A review. *IEEE Sensors Journal*, 22(3), 1807–1826.

Wolf, I.J. and Marquardt, W. (2016). Fast nmpc schemes for regulatory and economic nmpc – a review. *Journal of Process Control*, 44, 162–183.

Zhang, J., Yan, J., and Zhang, P. (2018). Fixed-wing uav formation control design with collision avoidance based on an improved artificial potential field. *IEEE Access*, 6, 78342–78351.

Zuo, Z., Liu, C., Han, Q.L., and Song, J. (2022). Unmanned aerial vehicles: Control methods and future challenges. *IEEE/CAA Journal of Automatica Sinica*, 9(4), 601–614.